ACS OMEGA

http://pubs.acs.org/journal/acsodf

Article

Effect of Exhausted Coffee Ground Particle Size on Metal Ion Adsorption Rates and Capacities

Elizabeth H. Gora, Samuel G. Saldana, Lauren M. Casper, Victor Coll Sijercic, Olga A. Giza, and Rebecca L. Sanders*

Cite This: *ACS Omega* 2022, 7, 38600−38612

Read Online

ACCESS | Metrics & More | Article Recommendations | Supporting Information

ABSTRACT: Spent coffee grounds (SCGs) are common waste products that can be used as low-cost adsorbents to remove contaminants from water. SCGs come in a range of particle sizes based on how they were ground to brew coffee. However, few studies have investigated how SCG particle size influences the adsorption rate and capacities of metal ions. In this study, SCGs were washed under alkaline conditions, creating exhausted coffee grounds (ECGs). ECGs were sieved into four particle size ranges (106−300, 300−500, 500−710, and 710−1000 μm). Mono-component batch adsorption experiments were conducted with each size fraction using 0.3 mM Pb^{2+}, Cu^{2+}, Zn^{2+}, and Ni^{2+} at pH 5.5 to examine the effect of particle size on the adsorption rates and capacities. The initial adsorption rates for all the four metal ions were 8−12 times higher for the smallest ECGs compared to the largest ECGs. Slower initial adsorption rates with increasing particle size were due to intraparticle diffusion of metal ions into the porous structure of ECGs. However, the equilibrium adsorption capacities for each metal ion and the surface acidic group concentrations were similar across the range of particle sizes studied, suggesting that grinding ECGs does not substantially change the number of adsorption sites. The equilibrium adsorption capacities for Cu^{2+} and Pb^{2+} were 0.18 and 0.17 mmol g^{-1}, respectively. Zn^{2+} and Ni^{2+} had lower adsorption capacities of 0.12 and 0.10 mmol g^{-1}, respectively. The time needed to reach equilibrium ranged from less than 2 h for Zn^{2+} and Ni^{2+} adsorption onto the smallest ECGs to several hours for Pb^{2+} or Cu^{2+} adsorption onto the largest ECGs. Future adsorption studies should consider the effect of ECG particle size on reported adsorption capacities, particularly for shorter experiments that have not yet reached equilibrium.

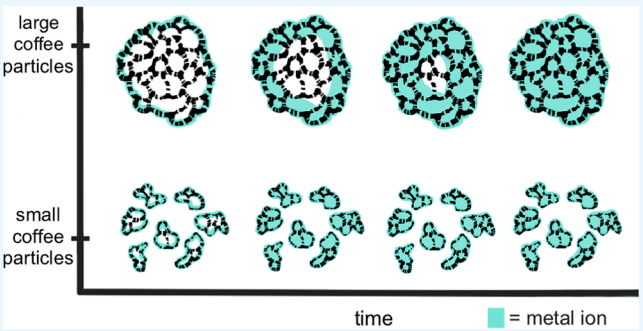

INTRODUCTION

Heavy metal ions such as Pb^{2+}, Cu^{2+}, Zn^{2+}, and Ni^{2+} can contaminate water from natural and anthropogenic sources such as mining, industrial, and agricultural activities.[1−3] These metal ions are toxic and do not readily degrade in the environment. Metal ions can be removed from water with adsorbents such as activated carbon,[4] commercial resins,[5] charcoal,[6] bone char, silica,[7] clay,[8] banana peels,[9] tea leaves,[10] and coffee waste.[11] Coffee production yields several forms of waste including used coffee grounds, typically referred to as spent coffee grounds (SCGs). Almost 170 million bags of coffee (10.2 million metric tons of beans) were consumed in 2020,[12] providing large quantities of SCGs that can be repurposed as economical adsorbents for water treatment.[13,14] SCGs are porous, lignocellulosic materials that have already been shown to have good adsorption capacities for metal ions (Table 1). Moreover, SCGs have also been shown to have excellent reusability with more than 90% of their adsorption capacity retained through multiple adsorption−desorption cycles using acidic conditions (pH ≤ 2) for regeneration.[15−17]

The adsorption rates and capacities of metal ions onto SCGs depend on variables such as adsorbent preparation, initial solution concentration, adsorbent dose, pH, contact time, temperature, and particle size.[11,14] Unlike many biosorbents, SCGs are already ground into different particle sizes depending on the desired brew for coffee consumption. For example, drip coffee requires medium to coarse particles that are approximately 600−1200 μm while espresso and Turkish coffee require finer particles that are 200−600 μm.[18] While many adsorption experiments report the particle size of SCGs,[9,15,16,19−22] only a few studies have considered particle size as a variable for adsorption capacities, producing contradictory findings.[23−26] Adsorption capacities have been reported to be higher for smaller coffee grounds compared to

Received: June 28, 2022
Accepted: September 19, 2022
Published: October 17, 2022

Table 1. Highest Reported Equilibrium Adsorption Capacities for Coffee Ground Adsorbents[a]

ion	coffee type	particle size (μm)	initial concentration (mM)	pH	contact time (min)	solid to solution (g L^{-1})	adsorption capacity (mmol g^{-1})	Reference
Pb^{2+}	exhausted	NR	≤0.291	5	overnight	0.971	0.0724	32
	spent	1000−2000	≤1.45	5	360	40	0.079	9
	coffee ground	NR	0.19	5	steady state	2.5	0.111	33
	untreated residues	<150	0.386	5	180	2	0.127	19
	exhausted	1000−710	0.3	5.5	240	1	0.168	this study
	exhausted	<1000	≤0.20	5	overnight	3	0.239	16
	spent	NR	≤1.2	4	7200	1.25	0.24	34
	activated exhausted	<75	0.48	6	75	1.5	0.297	35
	spent	NR	≤1.0	4.5	overnight	5	0.32	17
	modified	833	≤2.7	5	7200	1	0.59	36
	modified	NR	≤1.2	4	7200	1.25	0.77	34
Cu^{2+}	exhausted	<1000	≤0.20	5	overnight	3	0.0306	16
	exhausted	NR	≤0.291	5	overnight	0.971	0.0479	32
	exhausted	1000−710	0.3	5.5	240	1	0.184	this study
	spent	NR	≤4.72	5	7200	2.5	0.19	34
	spent	NR	≤1.0	4.5	overnight	5	0.21	17
	spent	<500	≤1.0	4.5	90	1	0.216	21
	modified	833	≤1.6	5	7200	1	0.73	36
	modified	NR	≤4.72	5	7200	2.5	1.53	34
Zn^{2+}	exhausted	NR	≤0.291	5	overnight	0.971	0.0483	32
	exhausted	<1000	≤0.20	5	overnight	3	0.0575	16
	untreated residues	<150	0.31	5	180	2	0.070	19
	spent (washed)	NR	≤2.29	5	180	10	0.082	1
	exhausted	1000−710	0.3	5.5	180	1	0.119	this study
	spent (unwashed)	NR	≤2.29	5	180	10	0.156	1
	aged CG biochar	<149	0.76	NR	720	1	0.347	37
	biochar from SCG	NR	0.1−5	5	240	25	0.526	38
Ni^{2+}	spent	1000−2000	≤5.11	5	360	40	0.039	9
	spent (washed)	NR	≤2.56	5	180	10	0.074	1
	treated exhausted	250−450	2.12	5	60	6.7	0.077	22
	exhausted	1000−710	0.3	5.5	180	1	0.102	this study
	spent (unwashed)	NR	≤2.56	5	180	10	0.128	1
	AC from SCG	NR	0.5−2.0	6	1440	0.8	0.884	39

[a]Values that were not reported are listed as NR.

larger coffee grounds after 60 min. For instance, Pb^{2+} adsorption experiments after 60 min indicated a 9% greater removal of Pb^{2+} from solution for coffee grounds less than 200 μm compared to coffee grounds greater than 200 μm.[23] Similarly, Sr^{2+} adsorption onto SCGs ranging from 100 to 900 μm concluded that finer particles had about 2.5% more uptake than coarser particles after 60 min.[24] Moreover, Fe^{2+} adsorption was 37.1% higher for 210−355 μm SCGs compared to 500−645 μm grounds after 60 min.[25] Although finer coffee grounds have been shown to reach equilibrium with metal ions such as Cd^{2+} within 60 min,[27] many adsorption experiments with SCGs report that equilibrium is not reached until 120 or 180 min.[1,10,26,28] One study that investigated SCG particle size with 240 min adsorption experiments reported that particle size did not have an effect on Cd^{2+} adsorption capacities.[26] From this review of the literature, we hypothesized that smaller coffee grounds have faster adsorption rates than larger coffee grounds, causing smaller particles to have higher adsorption capacities at shorter reaction times. Other biosorbents with smaller particle sizes have faster adsorption rates of metal ions;[29−31] however, no studies to our knowledge compared metal ion adsorption rates based on particle size for SCGs.

The goal of this work was to determine the adsorption rates and capacities for four metal ions onto different particle sizes of coffee grounds. SCGs were washed under alkaline conditions to remove soluble organic compounds producing exhausted coffee grounds (ECGs).[16,17,21,22,32] Monocomponent batch experiments were conducted with four heavy metal ions (Pb^{2+}, Cu^{2+}, Zn^{2+}, and Ni^{2+}) adsorbing onto ECGs that were separated into four particle size ranges representative of common particle sizes of used coffee grounds: 106−300, 300−500, 500−710, and 710−1000 μm. The equilibrium adsorption capacities and initial adsorption rates were quantified and compared. Differences in initial adsorption rates across the particle size ranges investigated were explained using an intraparticle diffusion model coupled with images of Pb^{2+} adsorption to the ECGs using scanning electron microscopy.

RESULTS AND DISCUSSION

Characterization of ECGs. ECGs were prepared by washing SCGs under alkaline conditions and sieving them

https://doi.org/10.1021/acsomega.2c04058
ACS Omega 2022, 7, 38600−38612

into four different particle size ranges. The smallest fraction was 106−300 μm, the middle fractions were 300−500 and 500−710 μm, and the largest fraction was 710−1000 μm. The surface morphology was identified with backscattered electron imaging using scanning electron microscopy (SEM) for each of the four size fractions (Figure 1). These images verified that

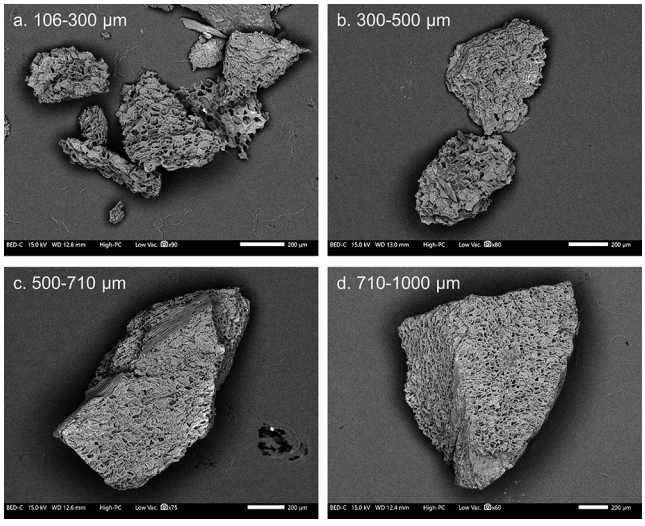

Figure 1. Backscattered electron images collected of ECGs representing particles from the size ranges of 106−300 μm (a), 300−500 μm (b), 500−710 μm (c), and 710−1000 μm (d). Scale bars represent 200 μm.

sieving separated most of the ECGs into appropriate size fractions. It is worth noting that when coffee is ground, a variety of shapes are formed, yielding heterogeneity in the particles associated with each size fraction. For example, Figure 1a clearly shows that the 106−300 μm size fraction includes a range of shapes and sizes. Backscattered electron images confirmed that the microstructure of ECGs was a porous network (Figure 1). When coffee is roasted, CO_2 and other gases are formed, which cause internal pressure that makes the roasted coffee crack and develop pores associated with evacuated cells.[40−42] Macropores are developed, which are 20−40 μm in size. An extensive network of macropores is visible in the images of the larger size fractions (Figure 1c,d); however, it is clear that grinding coffee into finer particles destroys many of the macropores from the originally roasted beans and increases the external surface area (Figure 1a,b).[42] In addition to macropores, ECGs also contain nanometer-sized pores called mesopores (2−50 nm) that would not be visible with SEM but provide a substantial surface area for adsorption.[43]

The functional groups associated with the ECG structure were characterized with attenuated total reflectance Fourier transform infrared (ATR-FTIR) spectroscopy. Each of the unreacted particle sizes produced similar spectra with absorption bands representing the lignocellulosic material found in coffee.[1,21,24,41,44−46] A broad peak around 3300 cm^{-1} is mainly attributed to the O−H stretching vibration with a minor contribution from the N−H stretching vibration (Figure 2a). Sharp peaks at 2923 and 2853 cm^{-1} represent asymmetric and symmetric C−H stretching vibrations. At 1743 cm^{-1}, a sharp peak represents a carbonyl stretching vibration, likely from polysaccharides, hemicellulose, and aliphatic esters.[41,45] A peak at 1648 cm^{-1} represents C═C vibrations found in lipids and fatty acids.[41] The fingerprint region below 1600 cm^{-1} contains a variety of peaks representing vibrations such as C−H, C−O, C−N, and P−O vibrations that are difficult to assign.[47]

The ECG surfaces were characterized with Boehm titrations to quantify acidic surface groups and with a batch equilibrium method to determine the pH values of the point of zero charge (Table 2).[39,48−50] Acidic surface groups were quantified by

Table 2. Chemical Composition of ECG Surfaces

size fraction (μm)	pH_{PZC}	total acidic groups (mequiv g^{-1})	lactone and carboxyl groups (mequiv g^{-1})	hydroxyl groups (mequiv g^{-1})
106−300	4.7	0.66	0.40	0.25
300−500	5.0	0.60	0.45	0.15
500−710	5.5	0.52	0.29	0.23
710−1000	5.5	0.58	0.37	0.21

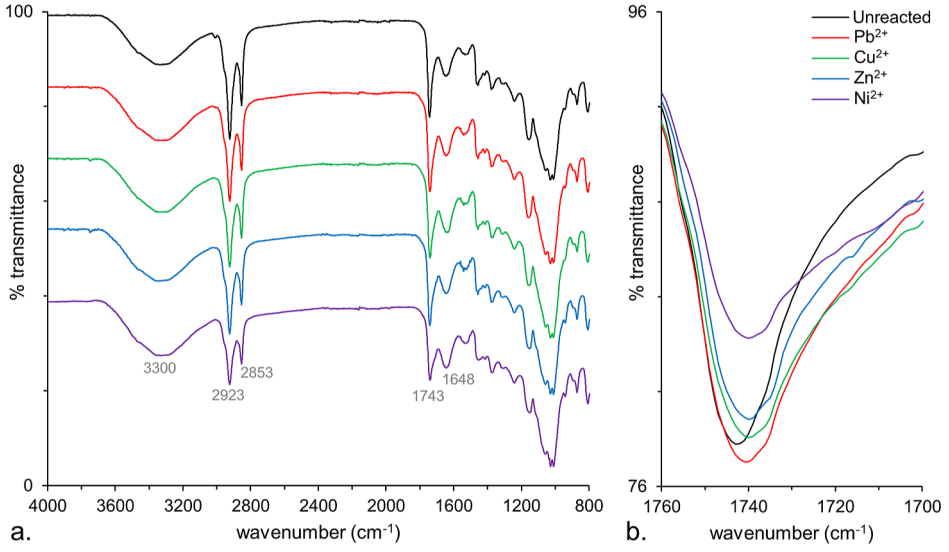

Figure 2. Representative FTIR spectra with ATR correction for 106−300 μm ECGs before and after Pb^{2+}, Cu^{2+}, Zn^{2+}, or Ni^{2+} adsorption (a). The carbonyl stretch around 1740 cm^{-1} shifts to slightly lower wavenumbers upon adsorption of each metal ion (b).

https://doi.org/10.1021/acsomega.2c04058
ACS Omega 2022, 7, 38600−38612

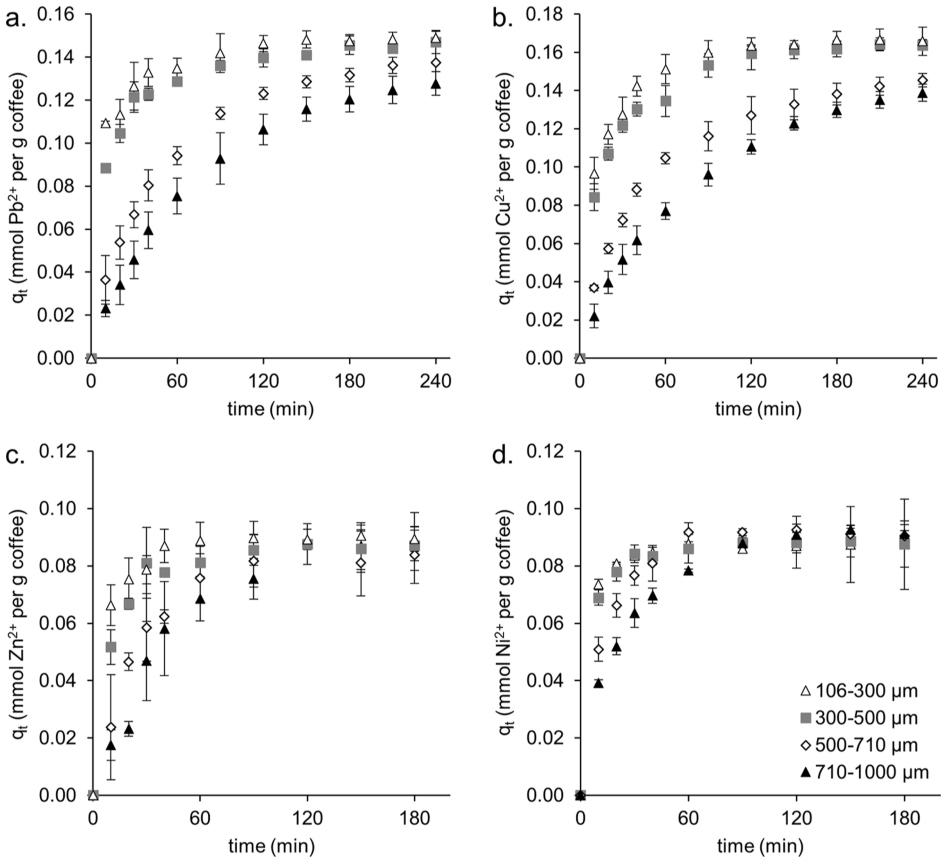

Figure 3. Adsorption curves for 0.3 mM Pb^{2+} (a), Cu^{2+} (b), Zn^{2+} (c), and Ni^{2+} (d) from monocomponent adsorption experiments onto ECGs. Error bars are standard deviations from replicate measurements.

Table 3. Parameters for Kinetic Models Including Pseudo-First-Order Rate Law Constants (k_1), Pseudo-Second-Order Rate Law Constants (k_2), Calculated Adsorption Capacities at Equilibrium (q_e), and Initial Adsorption Rates (ν_0) for 0.3 mM Metal Ions Adsorbed to Four Particle Size Ranges of ECGs

		pseudo-first order		pseudo-second order			
ion	particle size (μm)	k_1 (min^{-1})	R^2	k_2(g $mmol^{-1}$ min^{-1})	q_e(mmol g^{-1})	ν_0(mmol g^{-1} min^{-1})	R^2
Pb^{2+}	106−300	0.0108	0.907	1.08	0.1527	0.025	1.000
	300−500	0.0105	0.941	0.742	0.1512	0.0170	1.000
	500−710	0.0090	0.964	0.160	0.1606	0.00414	0.999
	710−1000	0.0074	0.977	0.0815	0.168	0.00231	0.996
Cu^{2+}	106−300	0.0103	0.857	0.660	0.1734	0.0199	1.000
	300−500	0.0098	0.905	0.457	0.1735	0.0137	0.999
	500−710	0.0075	0.960	0.159	0.1674	0.0044	1.000
	710−1000	0.0056	0.979	0.070	0.184	0.00238	0.998
Zn^{2+}	106−300	0.014	0.699	3.11	0.0920	0.026	1.000
	300−500	0.013	0.769	1.84	0.0903	0.015	0.999
	500−710	0.007	0.313	0.517	0.094	0.0046	0.996
	710−1000	0.005	0.429	0.152	0.119	0.0022	0.958
Ni^{2+}	106−300	0.014	0.567	6.76	0.0883	0.052	1.000
	300−500	0.015	0.738	4.52	0.0895	0.036	1.000
	500−710	0.013	0.593	1.58	0.096	0.014	0.998
	710−1000	0.0111	0.888	0.57	0.102	0.0059	0.998

reacting the ECGs with 0.05 M NaOH, which neutralizes phenolic, lactone, and carboxyl groups. Lactone and carboxyl groups were quantified by reacting the ECGs with 0.05 M Na_2CO_3. The phenolic group concentration was determined by taking the difference between the acidic group concentrations determined from reactions with NaOH and Na_2CO_3. The total acidic surface groups ranged from 0.52 to 0.66 mequiv g^{-1}. There were no clear trends in the concentrations of various acidic groups with respect to ECG particle size. Lactone and carboxyl groups were present in greater quantity compared to hydroxyl groups on the ECGs with concentrations ranging from 0.29 to 0.45 mequiv g^{-1} and from 0.15 to 0.25 mequiv g^{-1}, respectively (Table 2). Another study reported a comparable concentration of total acidic surface

https://doi.org/10.1021/acsomega.2c04058
ACS Omega 2022, 7, 38600−38612

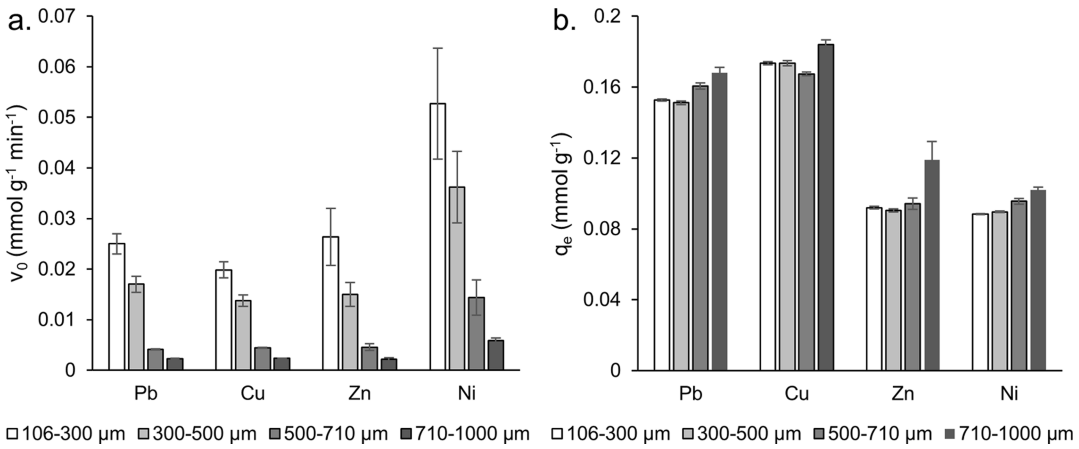

Figure 4. Initial adsorption rates (a) and equilibrium adsorption capacity (b) and for varying particle sizes of ECGs using 0.3 mM Pb^{2+}, Cu^{2+}, Zn^{2+}, and Ni^{2+} calculated from the linear form of the pseudo-second-order kinetic model. Error bars represent the standard error calculated from linear regression.

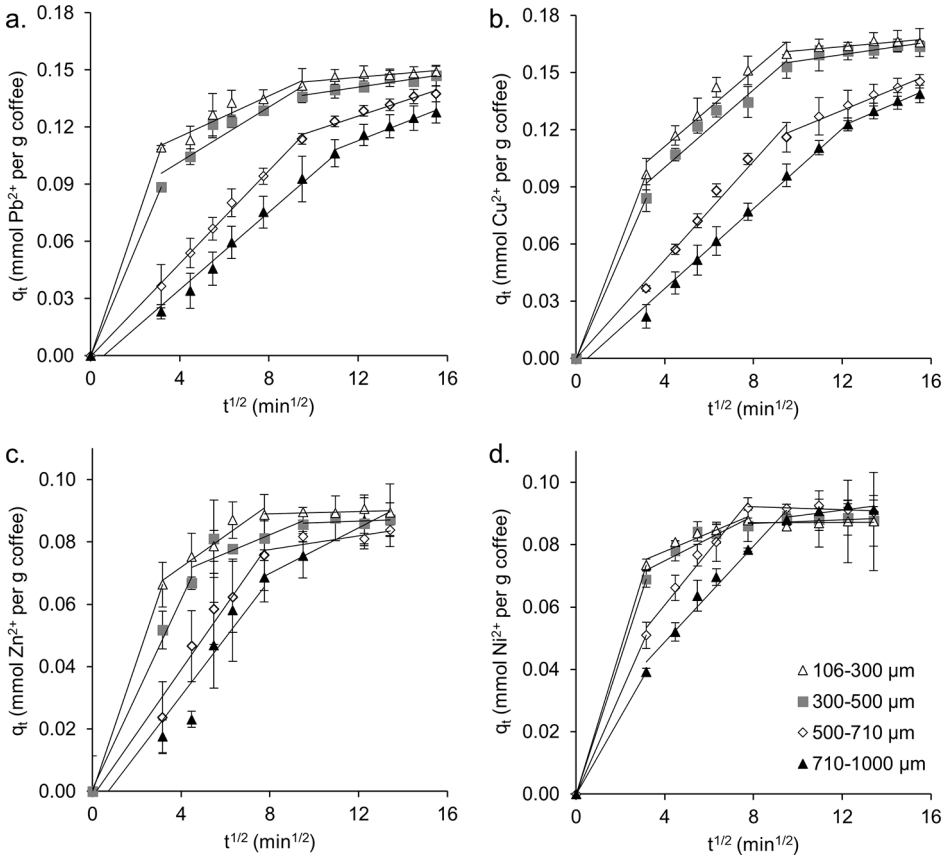

Figure 5. Intraparticle diffusion plots of adsorption capacity as a function of the square root of contact time for 0.3 mM Pb^{2+} (a), Cu^{2+} (b), Zn^{2+} (c), and Ni^{2+} (d). Error bars are standard deviations from replicate measurements.

groups on SCGs (0.75 mequiv g^{-1}); however, the SCGs had a higher concentration of hydroxyl groups compared to that of the carboxylic groups (0.52 and 0.23 mequiv g^{-1}, respectively).[21]

The pH values of the point of zero charge (pH_{PZC}) were determined to ensure that reactions were conducted with ECGs that would be able to attract positively charged metal ions. The pH_{PZC} values ranged from 4.7 for the smallest particles and 5.5 for the largest particles (Table 2 and Figure S1). Other studies have reported similar pH_{PZC} values for SCGs ranging from 4.5 to 5.65.[17,21,34,44] Previously, metal ion adsorption onto ECGs has been shown to be optimal under mildly acidic conditions (pH 4−6). At pH < 4, H^+ ions can compete for ion-exchange adsorption sites on coffee's surfaces, and at pH > 6, some metal ions can precipitate out as hydroxides.[10,21] A target pH of 5.5 was chosen for adsorption experiments so that the pH was high enough for ECG surfaces to potentially have a negatively charged surface to attract positively charged metal ions while keeping the pH low enough to prevent precipitation of metal ions from solution.

Adsorption Experiments. Adsorption curves were plotted for each monocomponent experiment of 0.3 mM Pb^{2+}, Cu^{2+},

https://doi.org/10.1021/acsomega.2c04058
ACS Omega 2022, 7, 38600−38612

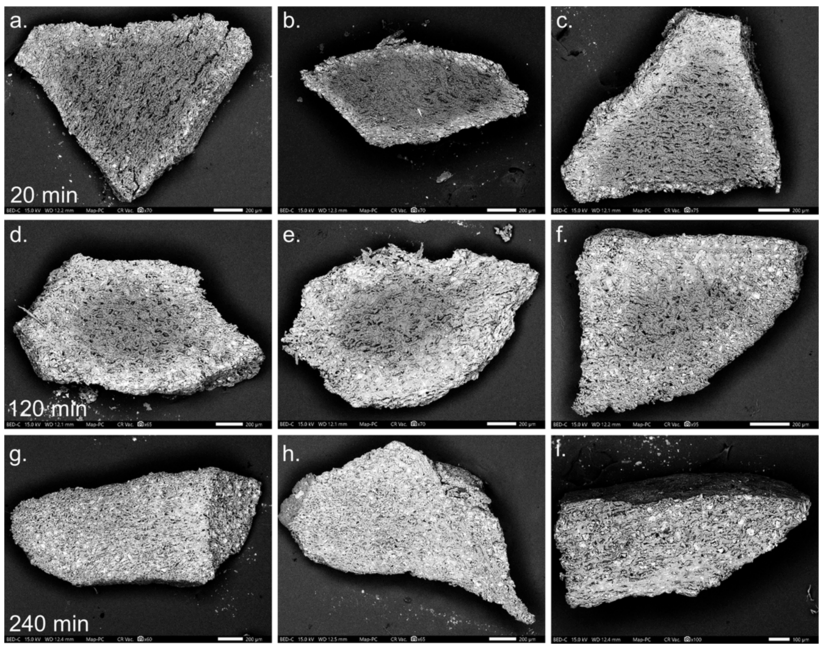

Figure 6. Backscattered electron images of cross sections of 710−1000 μm ECGs exposed to 0.3 mM Pb^{2+} for 20 (a−c), 120 (d−f), and 240 min (g−i). Brighter gray on the coffee grounds represents areas with higher concentrations of Pb^{2+}. Scale bars represent 200 μm. All images were collected with the same brightness and contrast for comparison between samples.

Zn^{2+}, and Ni^{2+} adsorbed to each particle size fraction of ECGs (Figure 3). The kinetic data was fit with the linear forms of the pseudo-first-order and pseudo-second-order kinetic models (eqs 1 and 2 detailed in the Materials and Methods section). Using these models, the adsorption capacities at equilibrium (q_e), the pseudo-first-order and pseudo-second-order rate law constants (k_1 and k_2), and the initial adsorption rates (ν_0) were calculated for each experimental condition (Tables 3 and S1 and Figure 4). The correlation coefficients (R^2) were compared for the two models with the pseudo-second-order model producing better fits ($0.958 < R^2 < 1.000$) than the pseudo-first-order model fits ($0.313 < R^2 < 0.979$) (Table 3 and Figures S2 and S3). Previous studies have also shown that the pseudo-second-order kinetic model well represents the adsorption kinetics of metal ions onto the surface of coffee.[19,26,34,51]

The intraparticle diffusion model proposed by Weber and Morris was used to assess the rate-limiting steps for adsorption by plotting adsorption capacity as a function of the square root of time. The resulting plots have one or more linear regions.[52] If the plot yields a straight line through the origin, the adsorption rate is limited by intraparticle diffusion. However, if two or three regions of linearity are observed, multiple stages of adsorption are present. Over 240 min of reaction time, two or three linear regions were observed for the ECGs (Figure 5).[53−55] For smaller particles, the first step was instantaneous adsorption onto the external surfaces of the ECGs.[54] The second step was gradual adsorption controlled by intraparticle diffusion. The third step was an equilibrium step as the contaminant migrates slowly from macropores to micropores.[55] For larger particles, the first step was not always present.

Effect of Particle Size on Pb^{2+} Adsorption Rates. The adsorption rates increased as the particle size decreased with the smallest ECGs adsorbing Pb^{2+} over 10 times faster initially than the largest ECGs (0.025 and 0.00231 mmol g^{-1} min^{-1}, respectively) (Table 2 and Figure 4a). The differences in initial adsorption rates were evaluated using the intraparticle diffusion model and backscattered electron images. When the adsorption capacity was plotted against the square root of time, the two larger size fractions only had two linear regions (Figure 5a). The first step associated with the first 120 min of the experiment was a straight line that almost goes through the origin, which implies that initial adsorption was limited by intraparticle diffusion.[56−58] The second linear region starting at 120 min was likely associated with diffusion into smaller pores.[53,59]

To confirm these assignments, the spatial distribution of Pb^{2+} over time was examined. Several 710−1000 μm ECGs exposed to 0.3 mM Pb^{2+} were removed at different adsorption times. They were cross-sectioned and imaged using backscattered electron imaging with X-ray mapping (Figures 6 and S4). At intermediate reaction times (e.g., 20 and 120 min for Pb^{2+}), higher concentrations of adsorbed Pb^{2+} were observed near the edges of the cross-sectioned ECGs (Figure 6a−f). At 20 and 120 min, the visible concentration of Pb^{2+} localized near the edges of the ECGs had average diffusion depths of 131 ± 43 μm and 262 ± 56 μm, respectively (Figure S5 and Table S2). Lower concentrations of Pb^{2+} were still observed in the center of the ECGs early in the experiment (Figure S4). It is possible that some Pb^{2+} ions migrated primarily through macropores into the center of the ECGs at short reaction times, but more time was needed for Pb^{2+} to saturate the adsorption sites found in mesopores. From 120 to 240 min, backscattered electron images indicate that intraparticle diffusion still takes place as a more uniform concentration of Pb^{2+} is observed throughout the ECGs by 240 min (Figures 6d−i and S4); however, the intraparticle diffusion model suggests the dominant adsorption mechanism shifts to diffusion into smaller pores (Figure 5a). By 240 min, adsorbed Pb^{2+} ions were found throughout the entire coffee particle (Figures 6g−i and S4). However, equilibrium was not yet

https://doi.org/10.1021/acsomega.2c04058
ACS Omega 2022, 7, 38600−38612

reached because the adsorption capacity had not yet plateaued (Figure 3a). Longer experiments on the largest ECGs indicated that Pb^{2+} adsorption continued slowly as Pb^{2+} migrated into smaller pores of the ECGs. Around 450 min, equilibrium was reached (Figure S6a), as determined by a third region of linearity in the intraparticle diffusion plot with a horizontal slope (Figure S6b).

For the two smaller size fractions, three linear steps were observed for the plot of adsorption capacity as a function of the square root of time (Figure 5a). Over half of the adsorption capacities were reached in the first 10 min. The steep initial slopes observed for the two smaller size fractions in Figure 5a suggest immediate adsorption onto the external surfaces of the ECGs.[54] The shallower slope from 10 to 90 min does not go through the origin, suggesting that intraparticle diffusion is not the sole rate-limiting step of Pb^{2+} adsorption for smaller ECGs. Since the average Pb^{2+} diffusion depths in larger ECGs were 131 ± 43 μm and 155 ± 35 μm at 20 and 40 min, respectively (Table S2), intraparticle diffusion into the smallest particles (<300 μm) should be relatively fast. Similarly, intraparticle diffusion was not observed to be a rate-limiting step for Pb^{2+} adsorption onto small coffee residues (<149 μm).[19] Instead, the linear region from 10 to 90 min suggests that adsorption is likely dominated by diffusion into the smaller pores of the ECGs (Figure 5a). After 90 min, a very shallow slope is observed, representing that the system slowly reaches equilibrium as Pb^{2+} adsorbs into the smallest pores of the ECGs.[55]

Effect of Particle Size on Pb^{2+} Adsorption Capacities. While adsorption rates varied markedly based on ECG particle size, adsorption capacities were similar across all particle sizes investigated (Figure 4b). At 240 min, the adsorption capacity for 0.3 mM Pb^{2+} was 17% higher for the smallest particles (0.149 mmol g^{-1}) compared to the largest particles (0.128 mmol g^{-1}). However, the calculated equilibrium adsorption capacity was 9% higher for the largest particles (0.168 mmol g^{-1}) compared to the smallest particles (0.153 mmol g^{-1}) (Table 3). Another study also found that particle size did not have an effect on the adsorption capacity of Cd^{2+} at 240 min for untreated coffee grounds.[26] Since the calculated equilibrium adsorption capacities for Pb^{2+} were similar across the particle size ranges investigated, this is likely due to the location of most adsorption sites on the ECGs. Smaller particles have more external surface area compared to larger particles, but the majority of adsorption sites on coffee grounds are associated on internal surfaces, particularly within mesopores.[43] Based on the backscattered electron images collected, Pb^{2+} is able to diffuse completely into the porous structure of even the largest ECGs over time. Therefore, our observations, in conjunction with the knowledge that most active sites are located in the mesopores of coffee, suggest that any increases in the external specific surface area of ECGs when crushed into smaller particles do not change substantially the available number of adsorption sites for ECGs. This would yield similar adsorption capacities across the particle size ranges studied.

The slightly higher calculated Pb^{2+} equilibrium adsorption capacity for the largest ECGs may be attributed to a challenge associated with the experimental setup. During batch adsorption experiments, some of the fine grounds (visually estimated to be 10−15% of all grounds) stuck to the sides of the container above the solution due to stirring or were lost when aliquots were removed and filtered over time. The small loss of grounds throughout the experiment may account for the slightly lower adsorption capacities calculated for the smaller grounds. However, we anticipate that adsorption capacities should be similar for different particle sizes if this experimental flaw was minimized. Overall, these Pb^{2+} adsorption experiments indicate that smaller ECGs have faster adsorption rates but similar adsorption capacities compared to larger ECGs.

Effect of Ion on Adsorption Rates. Adsorption experiments were conducted with 0.3 mM solutions of Cu^{2+}, Ni^{2+}, or Zn^{2+} to determine if other metal ions have similar adsorption properties compared to Pb^{2+} when exposed to ECGs of varying particle sizes. Cu^{2+}, Pb^{2+}, and Zn^{2+} had similar initial adsorption rates for each particle size (Figure 4a). For the largest particles, up to an 8% difference in initial adsorption rates was observed with Cu^{2+} having the fastest initial adsorption rate, followed by Pb^{2+} and Zn^{2+}. While the smallest particles had up to 31% difference in calculated initial adsorption rates (Zn^{2+} > Pb^{2+} > Cu^{2+}), the uncertainties in these calculated rates were large, suggesting minimal differences in rates between ions (Figure 4a and Table S1). The plots of adsorption capacity as a function of the square root of time for Cu^{2+} and Zn^{2+} were similar to Pb^{2+}, suggesting that all three had the same rate-limiting steps for adsorption based on particle size (Figure 5a−c).

The Ni^{2+} initial adsorption rates were 2−3 times faster than the other three ions investigated (Figure 4a). For example, the initial adsorption rates for the largest particles were 0.0058 and 0.0022 mmol g^{-1} min^{-1} for Ni^{2+} and Zn^{2+}, respectively. Similarly, for the smallest particles, the initial adsorption rates for Ni^{2+} and Cu^{2+} were 0.052 and 0.0199 mmol g^{-1} min^{-1}, respectively. The intraparticle diffusion model had three linear regions across all the four particle size ranges, suggesting an initial fast adsorption step even for larger particles (Figure 5d). The faster adsorption rates of Ni^{2+} compared to the other metal ions investigated have been reported previously for another biosorbent, sugar beet pulp. In their experiments, the adsorption rates onto sugar beet pulp particles (0.25−0.50 mm) were fastest for Ni^{2+}, followed by Zn^{2+}, Cu^{2+}, and Pb^{2+}.[60] The author suggested that the Ni^{2+} adsorption rates were higher because the only mechanism for adsorption for Ni^{2+} was ion exchange, whereas the other ions adsorbed more slowly because they also formed complexes with hydroxyl or carbonyl groups.[60]

Effect of Particle Size on Ion Adsorption Rates. Like Pb^{2+}, the initial adsorption rates for 0.3 mM Cu^{2+}, Ni^{2+}, and Zn^{2+} were 8−12 times faster onto the surfaces of the smallest ECGs compared to the largest ECGs (Table 3 and Figure 4a). For example, the initial adsorption rates for Cu^{2+} were 0.020 and 0.0024 mmol g^{-1} min^{-1} for the smallest and largest particle sizes, respectively. Similarly to Pb^{2+}, the slower adsorption rates for larger particles are likely due to the time it takes for the metal ions to diffuse into the ECGs. After 60 min, the adsorption capacities were higher for all the four ions for the smallest particles compared to the largest particles. For example, the adsorption capacity in 0.3 mM solutions at 60 min was 96% higher for Cu^{2+} for the smallest particle size compared to the largest particle size; it was only 12% higher for Ni^{2+} (Figure 3). The larger difference in Cu^{2+} adsorption capacities was due to slower initial adsorption rates compared to Ni^{2+} (Figure 4a). Higher adsorption capacities have been previously reported on smaller coffee grounds at 60 min for Pb^{2+}, Sr^{2+}, and Fe^{2+}.[23−25] By 90 min for Ni^{2+} and by 180 min for Zn^{2+}, the adsorption capacities were the same within the

https://doi.org/10.1021/acsomega.2c04058
ACS Omega 2022, 7, 38600−38612

error for the smallest and largest particles. This is in agreement with a study of cadmium(II) adsorption at pH 7 for 240 min that demonstrated that particles from 200 to 800 μm all had similar adsorption capacities.[26] Unlike Ni^{2+} and Zn^{2+}, the smallest particles had adsorbed 19% more Cu^{2+} or 17% more Pb^{2+} compared to the largest particles at 240 min. However, the calculated equilibrium adsorption capacities were 6−29% higher for the largest particle sizes compared to the smallest particle sizes for all the four ions studied (Figure 4b). Similar to Pb^{2+}, the adsorption capacities for the other metal ions do not vary greatly across the particle sizes investigated likely due to the similar number of active sites on a per gram basis for different particle sizes. Any observed increase in equilibrium adsorption capacity for larger particles compared to smaller particles is likely due to the previously discussed experimental flaw.

Adsorption Capacities Based on Ion. The highest equilibrium adsorption capacity, q_e, observed for each metal ion was compared to the published adsorption capacities on coffee adsorbents (Table 1). The equilibrium adsorption capacities for Cu^{2+}, Pb^{2+}, Zn^{2+}, and Ni^{2+} were 0.184, 0.168, 0.119, and 0.102 mmol g^{-1}, respectively, which all fell within the published ranges for adsorption capacities of each metal ion. In our experiment, q_e was the highest for Cu^{2+} and Pb^{2+}, followed by Zn^{2+} and Ni^{2+} (Figure 3b). Most studies comparing at least two of these metal ions found that Pb^{2+} had the highest adsorption capacity and Ni^{2+} had the lowest adsorption capacity.[9,16,17,19,32,34] Similarly, Reddad et al. demonstrated that the affinity order for sugar beet pulp (0.25−0.50 mm) was $Pb^{2+} > Cu^{2+} > Zn^{2+} > Ni^{2+}$.[60] A few reasons have been proposed for the higher affinities for Pb^{2+} and Cu^{2+}. For sugar beet pulp, higher adsorption capacities were reported for Pb^{2+} and Cu^{2+} because they both adsorbed via ion exchange and complexation, whereas Zn^{2+} and Ni^{2+} mostly or exclusively adsorbed via ion exchange. Moreover, Pb^{2+} and Cu^{2+} ions have higher first hydrolysis log K_1 (OH^-) constants than Zn^{2+} and Ni^{2+}, which lower the degree of solvation of Pb^{2+} and Cu^{2+} ions causing increased adsorption.[60−63]

Proposed Adsorption Mechanism. Adsorption experiments were conducted at pH 5.5. Since the pH_{PZC} value ranged from 4.7 to 5.5, the ECG surfaces had a negative or neutral charge, which could attract positively charged metal ions or allow for ion exchange with cations on the ECG surface (Table 2). The ATR-FTIR spectra and Boehm titrations of the ECGs indicated that several functional groups were present that could adsorb metal ions. The ATR-FTIR spectra for each ECG size fraction confirmed the presence of hydroxyl and carboxyl groups (Figure 2), which have been shown to be the key functional groups involved with Cu^{2+} and Pb^{2+} adsorption onto SCGs.[21,34] Previous studies have suggested that metal ions can interact with the surfaces of biosorbents via ion exchange and complexation with functional groups such as hydroxyl, carbonyl, and carboxyl groups.[1,21,34,60] Ion exchange is regularly cited as the dominant mechanism for metal ion adsorption of SCGs with the release of cations such as H^+ or Ca^{2+} into solution during adsorption.[1,34] During our batch adsorption experiments, H^+ ions were released into solution, as evidenced by decreasing pH values over time. Small aliquots of aqueous sodium hydroxide were added as needed to maintain a pH of 5.5. While the release of H^+ into solution was not quantified, the decreasing pH during experiments suggest that H^+ was exchanged for metal ions onto the surfaces of the ECGs. For these ECGs, the average quantity of acidic surface groups was 0.6 mequiv g^{-1} (Table 2). The largest calculated equilibrium adsorption capacity was 0.184 mmol g^{-1} for Cu^{2+} (0.368 mequiv g^{-1}), indicating that excess acidic surface groups were available to adsorb the metal ions (Table 3).

ATR-FTIR spectra were collected for each of the ECGs after metal ion adsorption (Figure 2a). While the spectra were similar to the spectra of unreacted ECGs, the carbonyl stretch at 1743 cm^{-1} slightly shifted to 1740 or 1741 cm^{-1}, and this feature broadened toward lower wavenumbers, suggesting changes to the carbonyl stretch as these sites adsorbed metal ions (Figure 2b). This shift was observed after adsorption for Pb^{2+}, Cu^{2+}, Zn^{2+}, and Ni^{2+}, suggesting that carboxyl groups were involved in adsorption for all the four metal ions investigated. There were at least 0.29 mequiv g^{-1} of carboxyl and lactone groups on each ECG size fraction. However, the calculated adsorption capacities of Cu^{2+} and Pb^{2+} were at least 0.33 and 0.30 mequiv g^{-1}, respectively. In some instances when the quantity of carboxyl and lactone groups was lower than the calculated absorption capacities, it is likely that the phenolic or hydroxyl group was also involved in adsorption.

Overall, this data supports previous findings that ion exchange is a likely mechanism for heavy metal ion adsorption onto ECGs.[1,34] Furthermore, there was no clear trend in terms of quantity of acidic surface groups on ECGs as a function of particle size (Table 2). This observation, in conjunction with the observed similarities in calculated adsorption capacities across particles sizes for a given ion, suggests that changes in particle size do not noticeably alter the adsorption mechanism for each metal ion (Figure 4b).

Effect of Particle Size on Adsorption Using Other Biosorbents. The effect of particle size on adsorption rates and capacities of metal ions has been explored for other biosorbents (Table S3). Similar to ECGs, smaller particle sizes of other biosorbents such as citrus peels, papaya seeds, and cassava peal waste adsorbed metal ions faster than larger particle sizes of the same biosorbent.[29−31,64] Smaller particles adsorb metal ions faster because of greater access to active sites on external surfaces and within pores. The adsorption capacities for smaller particles were generally greater than or equal to the adsorption capacities for larger particles. The adsorption capacities were typically higher for smaller particles when the contact time was 180 min or less. For example, smaller particle sizes of date seed powder[65] or cassava peel waste[29] were able to adsorb more Ni^{2+} after 30 or 180 min, respectively. Cd^{2+} removal was higher after 60 min for *Scolymus hispanicus*.[66] Similarly, the adsorption capacities for Cd^{2+} and Pb^{2+} were slightly higher for smaller papaya seeds after 120 min.[30] Moreover, smaller rice husk particles had higher adsorption capacities of Pb^{2+} in Cd^{2+} in column adsorption experiments.[67] Conversely, banana peel-based biosorbents of a range of particle sizes had similar adsorption capacities for Cu^{2+} after 1440 min.[68] The review of other biosorbents reinforces our observations of ECGs, suggesting that smaller particles adsorb metal ions faster. However, similar adsorption capacities can be achieved across a range of particle sizes if sufficient contact time is achieved.

Comparison of Adsorption Capacities to Other Adsorbents. The adsorption capacities of the ECGs were better than those of some biosorbents and activated carbons; however, many other biosorbents and commercial adsorbents have higher adsorption capacities (Table 4). The adsorption capacities of biosorbents derived from SCGs are influenced

https://doi.org/10.1021/acsomega.2c04058
ACS Omega 2022, 7, 38600−38612

Table 4. Comparison of Adsorption Capacities of Different Adsorbents

		q_e(mmol g^{-1})				
adsorbent	pH	Pb^{2+}	Cu^{2+}	Zn^{2+}	Ni^{2+}	reference
banana peel	5	0.03			0.087	9
water hyacinth	5	0.04			0.089	9
granular activated carbon	5	0.08	0.08			4
powdered activated carbon	5	0.13	0.07			4
AC cloths	5	0.147	0.174		0.152	73
ECG	5.5	0.168	0.184	0.119	0.102	this study
zeolite	5	0.54	0.27			4
modified corncob	4.8	0.57	0.67	0.44	0.62	5
Duolite GT-73	4.8	0.59	0.97	0.85	0.97	5
γ-Al_2O_3	4	0.60		0.90	1.42	74
algae	5	0.65	0.65			75
Dowex 50W strongly acidic cation-exchange resin	5	1.23	1.18			4
Amberlite IRC-718	4.8	1.4	2.0	2.4	2.2	5
Amberlite 200	4.8	1.7	1.4	1.3	1.5	5

by how the material is prepared. Several SCG preparations have been reported including using SCGs as is,[1,15,19,26,69] rinsing with water,[1,9,28] modifying with an acid or a base,[34,36,70] or pyrolyzing to form activated carbon.[39,43,71,72] In this study, ECGs were prepared by washing SCGs under alkaline conditions to remove soluble organic compounds that might have influenced any observed trends associated with adsorption rates or capacities due to changes in particle size. The adsorption capacities for each ion observed in this study were similar to values reported in the literature for coffee grounds used as is, washed with deionized water, or washed under alkaline conditions (Table 1). However, the adsorption capacities can be increased when used coffee grounds are chemically modified with acids or with pyrolysis (Table 1). There are trade-offs in terms of environmental and financial costs when using adsorbents derived from coffee waste. SCGs with minimal alterations have lower adsorption capacities but would be less expensive and have smaller ecological footprints. Activated carbon from SCGs has higher adsorption capacities; however, the energy consumed for carbonization would produce additional greenhouse gases.[14] For any preparation of SCGs, the porous structure of the material remains even if the surface chemistry, surface area, and pore sizes change. This work highlights the role of intraparticle diffusion for adsorption of metal ions into larger ECGs. The influence of intraparticle diffusion on adsorption rates and capacities should be considered for other preparations for SCG adsorbents and their subsequent use.

CONCLUSIONS

SCGs are readily available, low-cost adsorbents that come in a range of particle sizes. We have demonstrated when ECGs are prepared by washing SCGs under alkaline conditions and sieving into a range of particle sizes such hat smaller ECGs (106−300 μm) adsorb Pb^{2+}, Cu^{2+}, Zn^{2+}, and Ni^{2+} 8−12 times faster than larger ECGs (710−1000 μm). Slower initial adsorption rates for larger particles were linked to the time required for metal ions to diffuse into the porous structure of the ECGs. However, the equilibrium adsorption capacities and surface acidic group concentrations were similar across the particle size range, suggesting that grinding ECGs into smaller sizes does not substantially change the quantity of adsorption sites or the adsorption mechanism for these metal ions.

These observations are limited to batch experiments conducted with 0.3 mM solutions at pH 5.5, so more studies should consider if these trends are observed when other experimental parameters such as the type of the contaminant, SCG preparation, concentration, adsorbent dose, and pH are varied. The rate of uptake for metal ions on ECGs based on particle size may be an important variable to consider when scaling up this technology. For example, the faster adsorption rates of contaminants onto smaller ECGs may be desirable for packed bed systems because fluid may not have enough time to equilibrate with larger adsorbents as the solution flows through the column.[76,77] The few studies on metal ion adsorption onto SCGs and ECGs using fixed-bed column experiments did not investigate the effect of particle size in their studies.[16,78] Moreover, other studies have shown that ECGs can be regenerated, so how particle size influences the desorption rates of contaminants should also be explored.[15−17]

MATERIALS AND METHODS

Reagents. The reagents used were nitric acid (69.0−70.0%, Baker Instra-Analyzed Reagent, J. T. Baker), sodium hydroxide (ACS Grade, Research Products International), sodium nitrate (ACS reagent, Aldrich Chemical Company), sodium carbonate (98%, Alfa Aesar), lead(II) nitrate (99+%, ACS reagent, Aldrich), copper(II) nitrate hemi(pentahydrate) (98%, ACS reagent, Sigma-Aldrich), zinc(II) nitrate hexahydrate (reagent grade, 98%, Sigma-Aldrich), and nickel(II) nitrate hexahydrate (>99.0%). All solutions were prepared with deionized water.

Coffee Preparation. Arabica coffee beans were acquired from a farm near San Lucas Tolimán, Guatemala, through the North Central College Coffee Lab (Naperville, IL, USA). The beans were roasted to a medium roast before being ground with a conical burr coffee grinder using a very coarse or very fine setting. Roughly, 50 g of coarse grounds was brewed 5 times with 12 cups (2.8 L) of hot water using a standard drip coffee maker. Roughly, 65 g of fine grounds was brewed with 500 mL of boiling deionized water using a pour over funnel. This was repeated 15−20 times until the filtrate was a light golden color. Both size fractions were stirred with 0.01 M NaOH at 60 °C to leach soluble organic compounds and to allow greater access to more functional groups in hemicellulose such as hydroxyl and carboxyl groups.[16,21] After several washings, the solutions were mostly clear. The ECGs were rinsed with deionized water before suspension in 0.01 M HNO_3 until the pH was around pH 6. These washed ECGs were dried in an oven at 100 °C overnight and then sieved using ASTM sieves no. 18, 25, 35, 50, and 140 (1000, 710, 500, 300, and 106 μm, respectively). Four particle size ranges were used for further analysis: 1000−710, 710−500, 500−300, and 300−106 μm. Samples were stored in vacuum-sealed bags until further use.

Coffee Characterization. ECGs were characterized by FTIR spectroscopy before and after adsorption using a PerkinElmer Spectrum 100 with a universal attenuated total reflectance (ATR) accessory. A total of 64 scans were collected per sample with a resolution of 4 cm^{-1}. The surface morphology of each size fraction was determined by collecting images using a JCM-7000 benchtop scanning electron

https://doi.org/10.1021/acsomega.2c04058
ACS Omega 2022, 7, 38600−38612

microscope (JOEL USA Inc.) equipped with a tungsten filament source, an energy-dispersive X-ray detector, and a backscattered electron detector. All samples were mounted on aluminum stubs with adhesive carbon tabs and analyzed under low vacuum with a 15 kV acceleration voltage.

The pH of the point of zero charge (pH_{pzc}) was determined by preparing 25 mL solutions of 0.1 M $NaNO_3$ adjusted with NaOH or HNO_3 to achieve a range of initial pH values.[50] The initial pH was recorded before ECGs were added to each solution at a solid-to-solution ratio of 5 g L^{-1}. The solutions were shaken at 100 rpm overnight, and the final pH values were measured. The final pH was plotted as a function of initial pH. The pH_{PZC} values were determined where the final pH values plateaued on each plot.

The Boehm titration method was utilized to quantify acidic surface groups on the ECGs. Two grams of ECGs were added to glass bottles containing 50 mL of 0.05 M NaOH or 0.05 M Na_2CO_3. Nitrogen was bubbled over the solutions before the bottles were sealed and shaken overnight at 100 rpm. The solutions were filtered and 10 mL of the filtrate was back-titrated with 0.05 M HCl to neutralize excess base. The titrations were conducted in a nitrogen atmosphere eliminate interference from CO_2. Phenolic, lactone, and carboxyl groups were quantified using these titrations because NaOH reacts with all the three functional groups, whereas Na_2CO_3 reacts with lactone and carboxyl groups.[39,48,49]

Batch Adsorption Experiments. Batch adsorption experiments were conducted in triplicate using a solid-to-solution ratio of 1 g L^{-1}. All experiments were conducted with 0.3 mM metal ion solutions (20 ppm Cu^{2+}, Zn^{2+}, or Ni^{2+} or 60 ppm Pb^{2+}). This combination of initial concentration and solid-to-solution ratio was selected so that the calculated adsorption capacities should ideally be near the maximum adsorption capacity for each ion with the ECGs (Table 1). Experiments were conducted at room temperature (20−22 °C) with a target pH of 5.5 ± 0.2, which was controlled by adding microliter aliquots of aqueous NaOH or HNO_3 as needed. Chemical speciation calculations (Visual MINTEQ 3.1) indicated that each experiment had at least 98% of the initial ions present as the soluble divalent ion of interest, verifying minimal precipitation under these conditions (Tables S4−S7). The solutions were stirred at 400 rpm for up to 240 min. Stirring speeds above 200 rpm have not been shown to alter the adsorption rates.[21] At regular intervals, small aliquots (≤1 mL) were removed for elemental analysis. At the end of each experiment, coffee grounds were separated from the solutions via vacuum filtration, rinsed with minimal deionized water, and dried overnight at 60 °C before storing in vacuum-sealed bags until further analysis. While some preliminary adsorption experiments were conducted for up to 24 h, pH would drift overnight, resulting in unreliable results from longer experiments.

The solution concentrations over time were determined with flame atomic absorption spectroscopy. Elemental analysis for batch adsorption experiments using Cu^{2+}, Ni^{2+}, and Zn^{2+} was conducted using a PerkinElmer AAnalyst 300 flame atomic absorption spectrometer. Pb^{2+} concentrations were determined using a Shimadzu AA-7000 flame atomic absorption spectrometer. Adsorption curves were fit with the linear form of the pseudo-first-order kinetic model and the linear form of the pseudo-second-order kinetic model.[79,80] The equation for the linear form of the pseudo-first-order model is

$$\ln(q_e - q_t) = \ln q_e - k_1 t \quad (1)$$

where q_e is the adsorption capacity at equilibrium (mmol g^{-1}), q_t is the adsorption capacity at time t (mmol g^{-1}), k_1 is the pseudo-first-order rate constant (min^{-1}), and t is the time (min). The linear form of the pseudo-second-order kinetic model is

$$\frac{t}{q_t} = \frac{1}{k_2 q_e^2} + \frac{1}{q_e} t \quad (2)$$

where k_2 is the pseudo-second-order rate law constant (g $mmol^{-1}$ min^{-1}). The initial adsorption rate, ν_0, in units of mmol g^{-1} min^{-1}, is calculated as

$$\nu_0 = k_2 q_e^2 \quad (3)$$

Values for q_e and ν_0 were experimentally derived from the linear relationship of t/q_t as a function of t. The intraparticle diffusion model[52] was used to determine the effect of diffusion as the rate-controlling step of adsorption

$$q_t = k_p t^{1/2} + C \quad (4)$$

where k_p is the intraparticle diffusion rate constant (mol g^{-1} min^{-1}) found by plotting q_t as a function of $t^{1/2}$. C is a constant (mmol g^{-1}).

Scanning Electron Microscopy. Some of the 710−1000 μm samples with adsorbed Pb^{2+} were cut into cross sections with a thin razor to image where Pb^{2+} was present in the coffee grains over time (Figure 6). All samples were mounted on aluminum stubs with adhesive carbon tabs and analyzed under low vacuum with a 15 kV acceleration voltage using the JCM-7000 benchtop scanning electron microscope (JOEL USA Inc.) described above. ECGs with adsorbed Pb^{2+} were selected to image because of the higher adsorption capacities and the larger atomic mass of Pb^{2+}, both of which making it easier to collect backscattered electron images. Backscattered electron images were collected to determine compositional contrast for cross-sectioned samples after adsorption and energy-dispersive X-ray spectra were collected to determine the elemental composition of the cross-sectioned coffee grounds. Using the instrument's software, measurements were made on each image to estimate how far Pb^{2+} had readily diffused into the ECG structure over time (Figure S5 and Table S2). Preliminary images were also collected for cross sections of ECGs with adsorbed Cu^{2+}, Ni^{2+}, or Zn^{2+}; however, backscattered electron images and X-ray maps did not show the same contrast as Pb^{2+}-containing samples because the adsorbed concentrations were lower or the metal ions have lower atomic masses. A limited set of data (not shown) was collected with energy-dispersive X-ray spectroscopy of smaller areas either near the edges or the centers of cross-sectioned ECGs that indicated similar trends in adsorption compared to data collected for Pb^{2+}.

■ ASSOCIATED CONTENT

Supporting Information

The Supporting Information is available free of charge at https://pubs.acs.org/doi/10.1021/acsomega.2c04058.

Determination of pH at the point of zero charge, linear pseudo-first-order and pseudo-second-order fits, representative backscattered electron images with corresponding X-ray maps, measurements of Pb^{2+} depths over time into 710−1000 μm ECGs, kinetic data for longer Pb^{2+}

https://doi.org/10.1021/acsomega.2c04058
ACS Omega 2022, 7, 38600−38612

adsorption experiments, adsorption capacities of other biosorbents as a function of particle size, and chemical speciation calculations (PDF)

AUTHOR INFORMATION

Corresponding Author

Rebecca L. Sanders − *Department of Chemistry, North Central College, Naperville, Illinois 60540, United States;* orcid.org/0000-0002-7343-9087; Email: rlsanders@noctrl.edu

Authors

Elizabeth H. Gora − *Department of Chemistry, North Central College, Naperville, Illinois 60540, United States*

Samuel G. Saldana − *Department of Chemistry, North Central College, Naperville, Illinois 60540, United States*

Lauren M. Casper − *Department of Chemistry, North Central College, Naperville, Illinois 60540, United States*

Victor Coll Sijercic − *Department of Chemistry, North Central College, Naperville, Illinois 60540, United States*

Olga A. Giza − *Department of Chemistry, North Central College, Naperville, Illinois 60540, United States*

Complete contact information is available at: https://pubs.acs.org/10.1021/acsomega.2c04058

Notes

The authors declare no competing financial interest.

ACKNOWLEDGMENTS

The authors would like to acknowledge North Central College for funding this project. Jerry Thalmann of the North Central College Coffee Lab roasted the coffee for this study. McCrone Microscopes & Accessories, LLC (Westmont, Illinois), generously allowed the use of their scanning electron microscope and Glenn Miller of the McCrone Group assisted with sample preparation and collection of SEM images.

REFERENCES

(1) Ayala, J.; Fernández, B. Treatment of mining waste leachate by the adsorption process using spent coffee grounds. *Environ. Technol.* **2019**, *40*, 2037−2051.

(2) Duruibe, J. O.; Ogwuegbu, M. O. C.; Egwurugwu, J. N. Heavy metal pollution and human biotoxic effects. *Int. J. Phys. Sci.* **2007**, *2*, 112−118.

(3) Alengebawy, A.; Abdelkhalek, S. T.; Qureshi, S. R.; Wang, M. Q. Heavy Metals and Pesticides Toxicity in Agricultural Soil and Plants: Ecological Risks and Human Health Implications. *Toxics* **2021**, *9*, 42.

(4) An, H.; Park, B.; Kim, D. Crab shell for the removal of heavy metals from aqueous solution. *Water Res.* **2001**, *35*, 3551−3556.

(5) Vaughan, T.; Seo, C. W.; Marshall, W. E. Removal of selected metal ions from aqueous solution using modified corncobs. *Bioresour. Technol.* **2001**, *78*, 133−139.

(6) Karnib, M.; Kabbani, A.; Holail, H.; Olama, Z. Heavy metals removal using activated carbon, silica and silica activated carbon composite. *Energy Procedia* **2014**, *50*, 113−120.

(7) Yantasee, W.; Rutledge, R. D.; Chouyyok, W.; Sukwarotwat, V.; Orr, G.; Warner, C. L.; Warner, M. G.; Fryxell, G. E.; Wiacek, R. J.; Timchalk, C.; Addleman, R. S. Functionalized nanoporous silica for the removal of heavy metals from biological systems: adsorption and application. *ACS Appl. Mater. Interfaces* **2010**, *2*, 2749−2758.

(8) Yadav, V. B.; Gadi, R.; Kalra, S. Clay based nanocomposites for removal of heavy metals from water: A review. *J. Environ. Manage.* **2019**, *232*, 803−817.

(9) da Silva Correia, I. K.; Santos, P. F.; Santana, C. S.; Neris, J. B.; Luzardo, F. H.; Velasco, F. G. Application of coconut shell, banana peel, spent coffee grounds, eucalyptus bark, piassava (Attalea funifera) and water hyacinth (Eichornia crassipes) in the adsorption of Pb2+ and Ni2+ ions in water. *J. Environ. Chem. Eng.* **2018**, *6*, 2319−2334.

(10) Utomo, H. D.; Hunter, K. Adsorption of divalent copper, zinc, cadmium and lead ions from aqueous solution by waste tea and coffee adsorbents. *Environ. Technol.* **2006**, *27*, 25−32.

(11) Anastopoulos, I.; Karamesouti, M.; Mitropoulos, A. C.; Kyzas, G. Z. A review for coffee adsorbents. *J. Mol. Liq.* **2017**, *229*, 555−565.

(12) International Coffee Organization. Annual Review Coffee Year 2019/2020. https://www.ico.org/documents/cy2020-21/annual-review-2019-2020-e.pdf (accessed 6/21/2022).

(13) Chavan, A. A.; Pinto, J.; Liakos, I.; Bayer, I. S.; Lauciello, S.; Athanassiou, A.; Fragouli, D. Spent coffee bioelastomeric composite foams for the removal of Pb2+ and Hg2+ from water. *ACS Sustainable Chem. Eng.* **2016**, *4*, 5495−5502.

(14) Cerino-Córdova, F. J.; Dávila-Guzmán, N. E.; León, A. M. G.; Salazar-Rabago, J. J.; Soto-Regalado, E.Revalorization of coffee waste. *Coffee Prod. Res.***2020**, *133*. DOI: 10.5772/intechopen.92303

(15) Kyzas, G. Z. Commercial coffee wastes as materials for adsorption of heavy metals from aqueous solutions. *Materials* **2012**, *5*, 1826−1840.

(16) Utomo, H. D.; Hunter, K. Adsorption of heavy metals by exhausted coffee grounds as a potential treatment method for waste waters. *e-J. Surf. Sci. Nanotechnol.* **2006**, *4*, 504−506.

(17) Davila-Guzman, N. E.; Cerino-Córdova, F. d. J.; Loredo-Cancino, M.; Rangel-Mendez, J. R.; Gómez-González, R.; Soto-Regalado, E. Studies of adsorption of heavy metals onto spent coffee ground: equilibrium, regeneration, and dynamic performance in a fixed-bed column. *Int. J. Chem. Eng.* **2016**, *2016*, 9413879.

(18) Kruve Grind Size Reference. https://www.kruveinc.com/pages/brew-guide (accessed June 21, 2022).

(19) Wu, C.-H.; Kuo, C.-Y.; Guan, S.-S. Adsorption Kinetics of Lead and Zinc Ions by Coffee Residues. *Pol. J. Environ. Stud.* **2015**, *24*, 761.

(20) Seniūnaitė, J.; Vaiškūnaitė, R.; Bolutienė, V.Coffee grounds as an adsorbent for copper and lead removal form aqueous solutions. *The 9th International Conference "Environmental Engineering"*-22-23 May, 2014; pp 1−6.

(21) Dávila-Guzmán, N. E.; Cerino-Córdova, F. d. J.; Soto-Regalado, E.; Rangel-Mendez, J. R.; Díaz-Flores, P. E.; Garza-Gonzalez, M. T.; Loredo-Medrano, J. A. Copper biosorption by spent coffee ground: equilibrium, kinetics, and mechanism. *Clean: Soil, Air, Water* **2013**, *41*, 557−564.

(22) Liu, C.; Pujol, D.; Olivella, M. À.; de la Torre, F.; Fiol, N.; Poch, J.; Villaescusa, I.The role of exhausted coffee compounds on metal ions sorption. *Water, Air, Soil Pollut.***2015**, *226*(), 289. DOI: 10.1007/s11270-015-2568-2

(23) Seniūnaitė, J.; Vaiškūnaitė, R.; Bolutienė, V.Coffee grounds as an adsorbent for copper and lead removal form aqueous solutions. *The 9th International Conference " Environmental Engineering"*; VGTU Press, 2014.

(24) Imessaoudene, D.; Hanini, S.; Bouzidi, A. Biosorption of strontium from aqueous solutions onto spent coffee grounds. *J. Radioanal. Nucl. Chem.* **2013**, *298*, 893−902.

(25) Mohamed, K. N.; Yee, L. L. Removal of Fe Ion from Polluted Water by Reusing Spent Coffee Grounds. *Pertanika J. Sci. Technol.* **2019**, *27*, 1077.

(26) Azouaou, N.; Sadaoui, Z.; Djaafri, A.; Mokaddem, H. Adsorption of cadmium from aqueous solution onto untreated coffee grounds: equilibrium, kinetics and thermodynamics. *J. Hazard. Mater.* **2010**, *184*, 126−134.

(27) Delil, A. D.; Gülçiçek, O.; Gören, N. Optimization of adsorption for the removal of cadmium from aqueous solution using Turkish coffee grounds. *Int. J. Environ. Res.* **2019**, *13*, 861−878.

(28) Lavecchia, R.; Medici, F.; Patterer, S.; Zuorro, A. Lead removal from water by adsorption on spent coffee grounds. *Chem. Eng. Trans.* **2016**, *47*, 295−300.

(29) Kurniawan, A.; Kosasih, A. N.; Febrianto, J.; Ju, Y.-H.; Sunarso, J.; Indraswati, N.; Ismadji, S. Evaluation of cassava peel waste as

lowcost biosorbent for Ni-sorption: Equilibrium, kinetics, thermodynamics and mechanism. *Chem. Eng. J.* **2011**, *172*, 158−166.
(30) Gilbert, U. A.; Emmanuel, I. U.; Adebanjo, A. A.; Olalere, G. A. Biosorptive removal of Pb2+ and Cd2+ onto novel biosorbent: defatted Carica papaya seeds. *Biomass Bioenergy* **2011**, *35*, 2517−2525.
(31) Schiewer, S.; Balaria, A. Biosorption of Pb2+ by original and protonated citrus peels: Equilibrium, kinetics, and mechanism. *Chem. Eng. J.* **2009**, *146*, 211−219.
(32) Utomo, H. D.; Hunter, K. A. Particle concentration effect: adsorption of divalent metal ions on coffee grounds. *Bioresour. Technol.* **2010**, *101*, 1482−1486.
(33) Gomez-Gonzalez, R.; Cerino-Córdova, F. J.; Garcia-León, A. M.; Soto-Regalado, E.; Davila-Guzman, N. E.; Salazar-Rabago, J. J. Lead biosorption onto coffee grounds: Comparative analysis of several optimization techniques using equilibrium adsorption models and ANN. *J. Taiwan Inst. Chem. Eng.* **2016**, *68*, 201−210.
(34) Cerino-Córdova, F. J.; Díaz-Flores, P. E.; García-Reyes, R. B.; Soto-Regalado, E.; Gómez-González, R.; Garza-González, M. T.; Bustamante-Alcántara, E. Biosorption of Cu (II) and Pb (II) from aqueous solutions by chemically modified spent coffee grains. *Int. J. Environ. Sci. Technol.* **2013**, *10*, 611−622.
(35) Naga Babu, A. N.; Reddy, D. S.; Kumar, G. S.; Ravindhranath, K.; Krishna Mohan, G. K. Removal of lead and fluoride from contaminated water using exhausted coffee grounds based biosorbent. *J. Environ. Manage.* **2018**, *218*, 602−612.
(36) Botello-González, J.; Cerino-Córdova, F. J.; Dávila-Guzmán, N. E.; Salazar-Rábago, J. J.; Soto-Regalado, E.; Gómez-González, R.; Loredo-Cancino, M. Ion exchange modeling of the competitive adsorption of Cu (II) and Pb (II) using chemically modified solid waste coffee. *Water, Air, Soil Pollut.* **2019**, *230*, 73.
(37) Ke, Y.; Cui, S.; Fu, Q.; Hough, R.; Zhang, Z.; Li, Y. F. Effects of pyrolysis temperature and aging treatment on the adsorption of Cd(2+) and Zn(2+) by coffee grounds biochar. *Chemosphere* **2022**, *296*, 134051.
(38) Mantonanaki, A.; Pellera, F.; Gidarakos, E.Use of biochar generated from spent coffee grounds for the removal of Zn (II) from Aqueous Sollutions. *Proceedings of the 14th International Conference on Environmental Science and Technology Rhodes*: Greece, 2015; pp 3−5.
(39) Rodiguez, M. H.; Yperman, J.; Carleer, R.; Maggen, J.; Dadi, D.; Gryglewicz, G.; Bruggen, B. v. d.; Hernández, J. F.; Calvis, A. O. Adsorption of Ni (II) on spent coffee and coffee husk based activated carbon. *J. Environ. Chem. Eng.* **2018**, *6*, 1161−1170.
(40) Schenker, S.; Handschin, S.; Frey, B.; Perren, R.; Escher, F. Pore structure of coffee beans affected by roasting conditions. *J. Food Sci.* **2000**, *65*, 452−457.
(41) Wang, N.; Lim, L. T. Fourier transform infrared and physicochemical analyses of roasted coffee. *J. Agric. Food Chem.* **2012**, *60*, 5446−5453.
(42) Wang, X.; Lim, L.-T. Effect of roasting conditions on carbon dioxide degassing behavior in coffee. *Food Res. Int.* **2014**, *61*, 144−151.
(43) Boonamnuayvitaya, V.; Chaiya, C.; Tanthapanichakoon, W.; Jarudilokkul, S. Removal of heavy metals by adsorbent prepared from pyrolyzed coffee residues and clay. *Sep. Purif. Technol.* **2004**, *35*, 11−22.
(44) Imessaoudene, D.; Hanini, S.; Bouzidi, A.; Ararem, A. Kinetic and thermodynamic study of cobalt adsorption by spent coffee. *Desalin. Water Treat.* **2016**, *57*, 6116−6123.
(45) Pujol, D.; Liu, C.; Gominho, J.; Olivella, M.; Fiol, N.; Villaescusa, I.; Pereira, H. The chemical composition of exhausted coffee waste. *Ind. Crops Prod.* **2013**, *50*, 423−429.
(46) Ballesteros, L. F.; Teixeira, J. A.; Mussatto, S. I. Chemical, functional, and structural properties of spent coffee grounds and coffee silverskin. *Food Bioprocess Technol.* **2014**, *7*, 3493−3503.
(47) Lyman, D. J.; Benck, R.; Dell, S.; Merle, S.; Murray-Wijelath, J. FTIR-ATR analysis of brewed coffee: effect of roasting conditions. *J. Agric. Food Chem.* **2003**, *51*, 3268−3272.
(48) Boehm, H. Some aspects of the surface chemistry of carbon blacks and other carbons. *Carbon* **1994**, *32*, 759−769.
(49) Boehm, H. P.Chemical identification of surface groups. *Advances in catalysis*; Elsevier, 1966; Vol. *16*, pp 179−274.
(50) Babić, B. M.; Milonjić, S. K.; Polovina, M. J.; Kaludierović, B. V. Point of zero charge and intrinsic equilibrium constants of activated carbon cloth. *Carbon* **1999**, *37*, 477−481.
(51) Berhe, S.; Ayele, D.; Tadesse, A.; Mulu, A. Adsorption efficiency of coffee husk for removal of lead (II) from industrial effluents: equilibrium and kinetic study. *Int. J. Sci. Res.* **2015**, *5*, 1−8.
(52) Weber, W. J., Jr; Morris, J. C. Kinetics of adsorption on carbon from solution. *J. Sanit. Eng. Div., Am. Soc. Civ. Eng.* **1963**, *89*, 31−59.
(53) Allen, S.; McKay, G.; Khader, K. Intraparticle diffusion of a basic dye during adsorption onto sphagnum peat. *Environ. Pollut.* **1989**, *56*, 39−50.
(54) de Franco, M. A. E.; de Carvalho, C. B.; Bonetto, M. M.; Soares, R.; Féris, L. A. Removal of amoxicillin from water by adsorption onto activated carbon in batch process and fixed bed column: kinetics, isotherms, experimental design and breakthrough curves modelling. *J. Cleaner Prod.* **2017**, *161*, 947−956.
(55) Wu, F.-C.; Tseng, R.-L.; Juang, R.-S. Initial behavior of intraparticle diffusion model used in the description of adsorption kinetics. *Chem. Eng. J.* **2009**, *153*, 1−8.
(56) Guibal, E.; Jansson-Charrier, M.; Saucedo, I.; Cloirec, P. L. Enhancement of metal ion sorption performances of chitosan: effect of the structure on the diffusion properties. *Langmuir* **1995**, *11*, 591−598.
(57) Ribas, M. C.; De Franco, M. A.; Adebayo, M. A.; Lima, E. C.; Parkes, G. M.; Feris, L. A. Adsorption of Procion Red MX-5B dye from aqueous solution using homemade peach and commercial activated carbons. *Appl. Water Sci.* **2020**, *10*, 154.
(58) Vaghetti, J. C.; Lima, E. C.; Royer, B.; Cardoso, N. F.; Martins, B.; Calvete, T. Pecan nutshell as biosorbent to remove toxic metals from aqueous solution. *Sep. Sci. Technol.* **2009**, *44*, 615−644.
(59) Mall, I. D.; Srivastava, V. C.; Agarwal, N. K. Removal of Orange-G and Methyl Violet dyes by adsorption onto bagasse fly ash—kinetic study and equilibrium isotherm analyses. *Dyes Pigm.* **2006**, *69*, 210−223.
(60) Reddad, Z.; Gerente, C.; Andres, Y.; Le Cloirec, P. Adsorption of several metal ions onto a low-cost biosorbent: kinetic and equilibrium studies. *Environ. Sci. Technol.* **2002**, *36*, 2067−2073.
(61) Burns, C. A.; Cass, P. J.; Harding, I. H.; Crawford, R. J. Adsorption of aqueous heavy metals onto carbonaceous substrates. *Colloids Surf., A* **1999**, *155*, 63−68.
(62) Martell, A. E.; Hancock, R. D.*Metal Complexes in Aqueous Solutions*; Springer Science & Business Media, 2013.
(63) Dzombak, D. A.; Morel, F. M.*Surface Complexation Modeling: Hydrous Ferric Oxide*; John Wiley & Sons, 1991.
(64) Schiewer, S.; Patil, S. B. Pectin-rich fruit wastes as biosorbents for heavy metal removal: equilibrium and kinetics. *Bioresour. Technol.* **2008**, *99*, 1896−1903.
(65) Elkhaleefa, A.; Ali, I. H.; Brima, E. I.; Elhag, A.; Karama, B. Efficient removal of Ni (II) from aqueous solution by date seeds powder biosorbent: adsorption kinetics, isotherm and thermodynamics. *Processes* **2020**, *8*, 1001.
(66) Barka, N.; Abdennouri, M.; Boussaoud, A.; Makhfouk, M. E. Biosorption characteristics of Cadmium (II) onto Scolymus hispanicus L. as low-cost natural biosorbent. *Desalination* **2010**, *258*, 66−71.
(67) Tarley, C. R. T.; Arruda, M. A. Z. Biosorption of heavy metals using rice milling by-products. Characterisation and application for removal of metals from aqueous effluents. *Chemosphere* **2004**, *54*, 987−995.
(68) Hossain, M. A.; Ngo, H. H.; Guo, W. S.; Nguyen, T. V. Biosorption of Cu (II) from water by banana peel based biosorbent: experiments and models of adsorption and desorption. *J. Water Sustainability* **2012**, *2*, 87−104.

https://doi.org/10.1021/acsomega.2c04058
ACS Omega 2022, 7, 38600−38612

(69) Kim, M.-S.; Kim, J.-G. Adsorption characteristics of spent coffee grounds as an alternative adsorbent for cadmium in solution. *Environments* **2020**, *7*, 24.
(70) Akindolie, M.; Choi, H. Surface modification of spent coffee grounds using phosphoric acid for enhancement of methylene blue adsorption from aqueous solution. *Water Sci. Technol.* **2022**, *85*, 1218−1234.
(71) Sukhbaatar, B.; Yoo, B.; Lim, J. H. Metal-free high-adsorption-capacity adsorbent derived from spent coffee grounds for methylene blue. *RSC Adv.* **2021**, *11*, 5118−5127.
(72) Block, I.; Günter, C.; Duarte Rodrigues, A.; Paasch, S.; Hesemann, P.; Taubert, A. Carbon Adsorbents from Spent Coffee for Removal of Methylene Blue and Methyl Orange from Water. *Materials* **2021**, *14*, 3996.
(73) Kadirvelu, K.; Faur-Brasquet, C.; Cloirec, P. L. Removal of Cu (II), Pb (II), and Ni (II) by adsorption onto activated carbon cloths. *Langmuir* **2000**, *16*, 8404−8409.
(74) Rahmani, A.; Mousavi, H. Z.; Fazli, M. Effect of nanostructure alumina on adsorption of heavy metals. *Desalination* **2010**, *253*, 94−100.
(75) Pagnanelli, F.; Esposito, A.; Vegliò, F. Multi-metallic modelling for biosorption of binary systems. *Water Res.* **2002**, *36*, 4095−4105.
(76) Hubbe, M. A.; Azizian, S.; Douven, S. Implications of apparent pseudo-second-order adsorption kinetics onto cellulosic materials: A review. *BioResources* **2019**, *14*, 7582.
(77) Sen Gupta, S.; Bhattacharyya, K. G. Kinetics of adsorption of metal ions on inorganic materials: A review. *Adv. Colloid Interface Sci.* **2011**, *162*, 39−58.
(78) Davila-Guzman, N. E.; Cerino-Córdova, F. d. J.; Loredo-Cancino, M.; Rangel-Mendez, J. R.; Gómez-González, R.; Soto-Regalado, E.Studies of adsorption of heavy metals onto spent coffee ground: equilibrium, regeneration, and dynamic performance in a fixed-bed column. *Int. J. Chem. Eng.***2016**, *2016*. DOI: 10.1155/2016/9413879
(79) Ho, Y. S. Second-order kinetic model for the sorption of cadmium onto tree fern: a comparison of linear and non-linear methods. *Water Res.* **2006**, *40*, 119−125.
(80) Ho, Y. S.; McKay, G. Sorption of dye from aqueous solution by peat. *Chem. Eng. J.* **1998**, *70*, 115−124.

https://doi.org/10.1021/acsomega.2c04058
ACS Omega 2022, 7, 38600−38612